Numerical Investigation of a General Cargo Vessel Wake in Waves

Mohsen Irannezhad, Arash Eslamdoost, and Rickard E. Bensow
Chalmers University of Technology, Gothenburg/Sweden
mohsen.irannezhad@chalmers.se

1 Introduction

Since calm water is rather an exception at an actual sea, optimizing propulsive efficiency of ships operating in more realistic environmental conditions than calm water has been gaining more attention recently. The effects of waves on propeller performance have been investigated by different researchers such as Taskar et al. (2016) who studied different influencing factors in terms of cavitation, pressure pulses and efficiency on propeller performance of KVLCC2. Since excessive wake variation in waves may have a significant impact on the propeller performance, it is important to study dynamics of the wake field for ships operating in waves.

Although the propeller designers consider experienced-based margins for propellers operating in waves and off-design conditions, the knowledge of the wake field at different wave conditions for each specific hull could be beneficial in designing more efficient propeller. In this study, a general cargo vessel incorporating a Large Diameter Propeller (LDP) with a very small tip clearance is considered. In an earlier investigation, the authors of the current paper have carried out a study, Irannezhad et. al. (2019), on the propeller emergence risk assessment of the LDP vessel employing a potential flow panel code, SHIPFLOW Motions, as well as a viscous flow solver, STAR-CCM+. The aim of this paper is to first validate the LDP vessel computed heave and pitch motions as well as its resistance due to regular head waves in model scale against the experimental data, then to analyze the time-varying wake field and compare it in different wave conditions in the viscous flow solver. The propeller is not modeled in the simulations.

2 Vessel geometry and conditions

An overview of the LDP vessel geometry with a tunnel-shaped aft design meant to accommodate an LDP is shown in Fig. 1 together with the ship-fixed coordinate system at the vessel Center Of Gravity (COG). A simple shaft connects the vessel bare hull to an appended asymmetric rudder. Although the LDP is not modeled in the simulations, its conceptual geometry is represented in Fig. 1. A point probe at the position of the LDP blade tip near the propeller/hull clearance is specified in order to characterize the propeller emergence in the absence of propeller in the simulations. The LDP vessel main particulars in model-scale, its speed as well as the corresponding Froude number are listed in Table 1.

Table 1: The model-scale LDP vessel main particulars and conditions (scale factor = 27).

Particular	≈ Value	Unit	Denotation
L_{pp}	7.95	[m]	Length Between Perpendiculars
LOS	8.11	[m]	Length Overall Submerged
B	0.88	[m]	Breadth at mid-ship
T_A	0.296	[m]	Draft at Aft Perpendicular
T_F	0.296	[m]	Draft at Fore Perpendicular
Δ	1740	[kg]	Mass Displacement
V	0.89	$[\frac{m}{s}]$	Model Speed
Fr	0.10	[-]	Froude Number
Re	7.1E6	[-]	Reynolds Number

Fig. 1: LDP vessel geometry, point probe and ship-fixed coordinate system at COG.

The model-scale LDP vessel appended with a rudder and a shaft, free to heave and pitch operating in fresh water with the density of $\rho = 998.3\ \frac{kg}{m^3}$ is used within the numerical investigations. The simulations are performed in calm water and in the 5^{th} order Stokes regular head waves ($\mu = 180°$) in deep water as listed in Table 2. On the other hand, the LDP vessel model-tests were conducted in free-running self-propulsion mode by Maritime Research Institute Netherlands (MARIN). Fast Fourier Transform (FFT) analysis is used in order to post-process the experimental and numerical data.

Table 2: Environmental conditions of the studied cases.

Case no.	Cond.	$\approx H$ **[m]**	$\approx \lambda$ **[m]**	$\approx \frac{\lambda}{LOS}$ **[-]**	$\approx$ **Steepness** $= \frac{H}{\lambda}$ [-]	$\approx \omega_e\ [\frac{rad}{s}]$	$\approx T_e\ [s]$
1	Calm	-	-	-	-	-	-
2	Wave	0.22	5.57	0.68	0.039	4.33	1.45
3	Wave	0.22	7.27	0.89	0.030	3.68	1.70

The total resistance R_T in self-propulsion model tests is estimated based on the mean measured thrust $\bar{T}$ and the given calm water thrust deduction factor of $t_d = 0.159$ at Froude number 0.10 , see Eq. 1. It is assumed that the thrust deduction factor in waves is equal to that of calm water, t_d.

$$R_T = (1 - t_d) \times \bar{T}. \tag{1}$$

3 Numerical modeling

The CFD simulations are performed using an URANS approach. A second order spacial discretization scheme is used. In order to simulate the vessel motions, the Dynamic Fluid Body Interaction (DFBI) module is used. The DFBI Rotation and Translation model is used in order to enable the RANS solver to compute the vessel motions from the exciting fluid forces and moments as well as the gravity force. The Planar Motion Carriage mechanism is used within the DFBI Rotation and Translation model, in order to simulate the hull free to heave and pitch (2 degrees of freedom) while it is translating with a prescribed constant speed (ship forward speed V) in the longitudinal direction in the earth-fixed co-ordinate system. In order to achieve a robust simulation setup for wave propagation in STAR-CCM+, the best practice provided by Peric' (2017) is complied. The aim is to minimize the wave propagation simulation issues, such as amplitude reduction and period change during propagation, disturbances (wiggles) on the free-surface and reflection at boundaries. The Volume of Fluid (VOF) multiphase model is used as the free-surface capturing technique. The High-Resolution Interface Capturing (HRIC) scheme by Muzaferija and Peric' (1999) is used in VOF simulations to maintain a sharp interface between the incompressible fluid phases.

Mesh generation was performed using the automatic mesh generation tool in STAR-CCM+. The trimmed hexahedral meshes with local refinements near the free-surface as well as near the hull together with prism layers along the hull surface are used. Overset method consisting a moving overset region and a stationary background region with specific treatment of cell sizes near the overlapping region is used to discretize the computational domain. The prism layers are placed in such a way that the non-dimensional wall distance y^+ remains above 30 over the major part of the hull surface during the simulation, hence

wall functions utilization. An overview of the background mesh is shown in Fig. 2 in which the applied boundary conditions is also given. The pressure outlet boundary condition for simulation in calm water is moved from the top boundary to the outlet boundary. Due to the asymmetric geometry of the rudder, no symmetry plane is considered and both side boundaries are given as velocity inlets. For simulations in waves, the wave forcing capability is applied to all of the vertical boundaries in order to force the solution of the discretized Navier-Stokes equations towards the theoretical 5^{th} order Stokes wave solution over a distance equal to Length Overall Submerged (LOS) from the boundaries. For simulation in calm water, the wave damping capability is used in all of the vertical boundaries in order to minimize the wave reflection from the boundaries. The Standard Low-Re $k-\varepsilon$ turbulence model and the Realizable $k-\varepsilon$ turbulence model together with all y^+ wall treatment are used for simulations in waves and calm water respectively. An implicit unsteady solver with a second order temporal discretizational scheme (time-step of 0.003 s) for simulation in waves and a first order temporal discretizational scheme (time-step of 0.02 s) for simulation in calm water is used. The chosen time-step also fulfills the ITTC (2011) recommended criteria of at least 100 time-steps per encountered wave period. Last but not least, ten and forty maximum number of inner iterations for each unsteady time-step is considered in simulations in waves and calm water respectively.

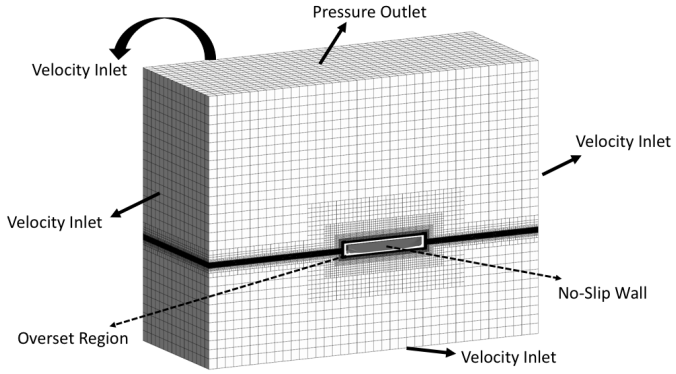

Fig. 2: An overview of the background mesh and the applied boundary conditions.

Table 3: Number of cells in each region.

Cond.	Background	Overset	Total
Calm	5.8 M	2.3 M	8.1 M
Wave	13.5 M	4.1 M	17.6 M

4 Resistance and motions validation

Due to a very small Froude number, the dynamic sinkage and trim as well as the wave making resistance in calm water attain very small values. The self-propelled model test sinkage, trim and total resistance are -0.003 [m], 0.017 [deg] and 15.8 [N], respectively, while the CFD results are -0.002 [m], 0.114 [deg] and 14.6 [N]. Positive sinkage and heave (R3) defined as COG moves upward and positive trim and pitch (R5) are defined as bow moves downward. The 0^{th} harmonic amplitudes of motions in simulations in waves are approximately similar and relatively small. Nevertheless, the 1^{st} harmonic amplitudes of heave and pitch motions, shown in Fig. 3, are the dominating components while higher order components are close to zero. The large amplitude heave response in Case 2 might be due to the near heave resonance conditions. The deviation errors of the 1^{st} harmonic amplitudes of motions and the 0^{th} harmonic amplitudes of resistance from the experimental data are presented on top of each bar in Fig. 3e and 3f. In general, a good agreement is seen between CFD and EFD data.

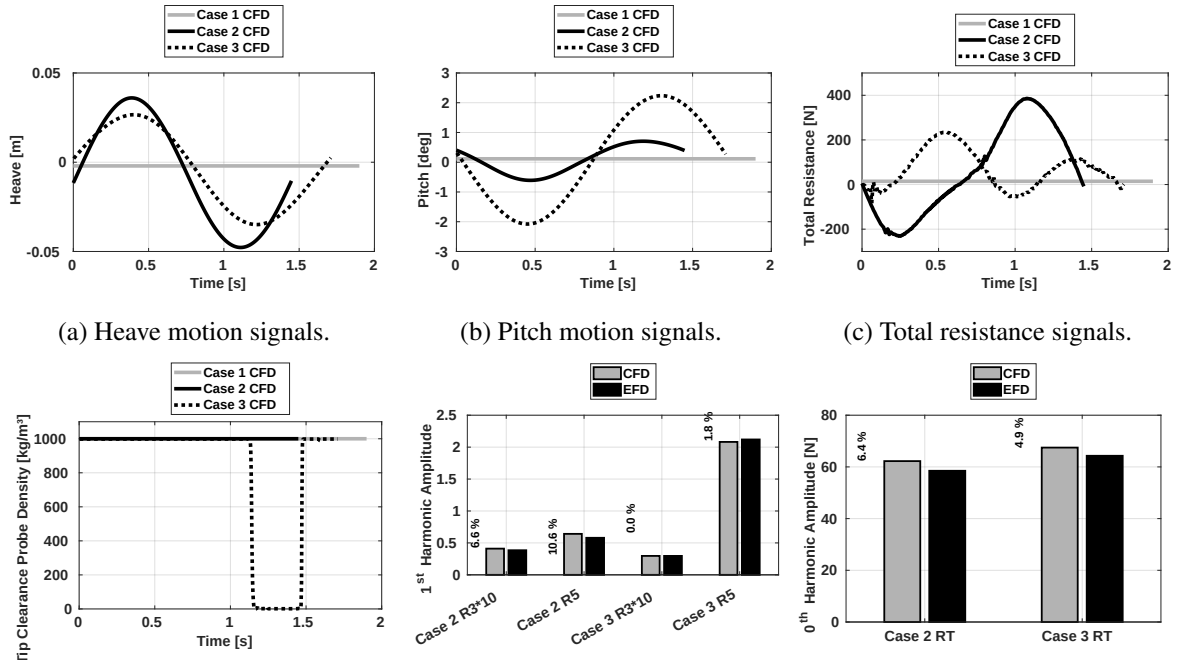

(a) Heave motion signals. (b) Pitch motion signals. (c) Total resistance signals.

(d) Probe density monitor. (e) Motions harmonic amplitudes. (f) Mean total resistance.

Fig. 3: The LDP vessel responses during one encountered wave period.

5 Propeller wake investigations

In this section the nominal wake variation in waves and in calm water is investigated for the LDP vessel. The wake has been studied on a virtual disk located at the propeller center and it is moving with the hull during the motion responses. The disk radius is equal to the propeller radius ≈ 0.13 m. The propeller disk is divided into 11 surfaces in radial direction, with the first surface starts at the shaft edge to a radius of $\Delta r_1 = 0.03m$ and the remaining 10 surfaces with the radius steps of $\Delta r_{2...11} = 0.01m$ to the propeller tip. The disk surface centers are also derived. The mean value of the surface averaged axial and radial velocity components during one encountered wave period is shown in the Fig. 7b and 7c at each surface center radius. The surface averaged calm water wake fraction as well as the surface averaged wake fraction variation during one encounter wave period for simulations in waves are shown in Fig. 7a. Significant wake variation in waves in comparison to calm water wake is seen. The computed values of the mean surface averaged wake fraction for Case 2 and Case 3 are approximately similar to the calm water value; however, a different distribution of the axial an radial velocity components are observed, see Fig. 7b and 7c. The sudden change of wake fraction in Case 3 between 1.12 s and 1.47 s is due to the propeller emergence shown in Fig. 3d. Strong correlation between the pitch motion and the wake field dynamics is seen. The wake fraction is at its minimum (meaning that the inflow velocity into the propeller disk is close to free stream velocity) when the pitch motion is close to zero and the hull stern is just about to move downwards into the water. On the other hand, the wake fraction is at its maximum when the pitch motion is zero but the hull stern moving upwards out of water. The non-dimensional axial velocity contour in the shaft direction as well as the transverse velocity vectors for the simulation in calm water is shown in Fig. 4. Moreover, the non-dimensional axial velocity contours and the transverse velocity vectors for three time instances of the lowest, the mean level and the highest surface averaged wake fraction for simulations in waves are shown in Fig. 5 and Fig. 6. The bilge vortex found by the same Q-criterion are shown in Fig. 8. The bilge vortices in waves show interesting dynamics in comparison to calm water. They become stronger by increasing wave length. The position where the bilge vortices hit the propeller disk in calm water is more and less stationary, while they considerably move up and down in the disk when the waves are present. The other interesting phenomenon in waves is the existence of the secondary vortex system which is caused by the propeller shaft and enters the propeller disk.

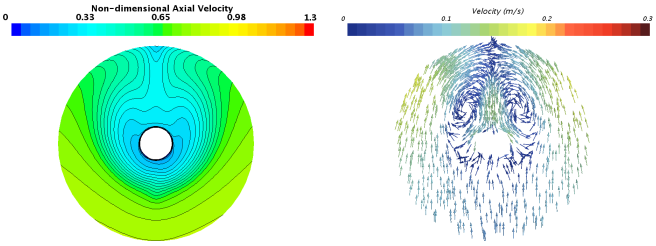

(a) Non-dim. axial contour. (b) Transverse vectors.

Fig. 4: Velocity components on the propeller disk in calm water (Case 1).

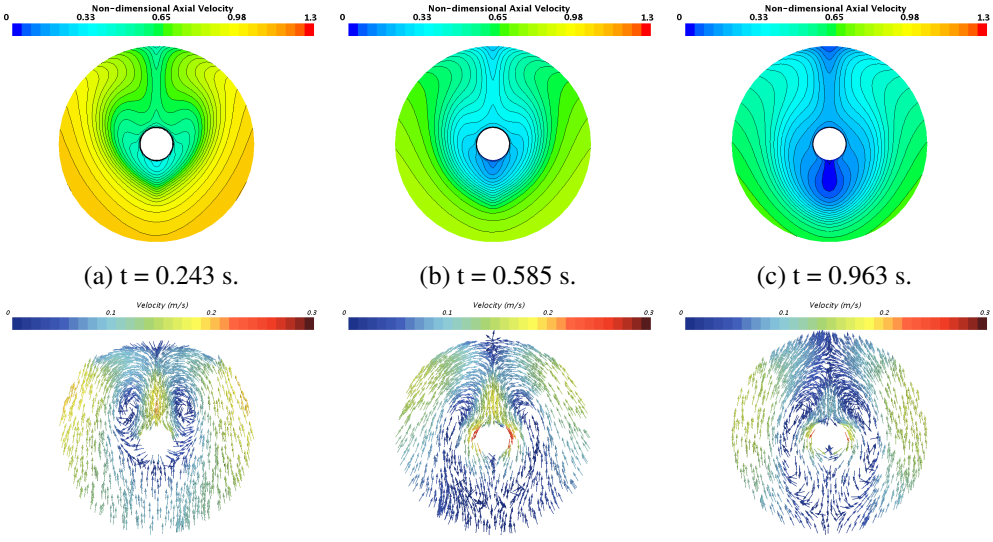

(a) t = 0.243 s. (b) t = 0.585 s. (c) t = 0.963 s.

(d) t = 0.243 s. (e) t = 0.585 s. (f) t = 0.963 s.

Fig. 5: Non-dimensional axial velocity contours and transverse velocity vectors for Case 2 at three time instances; wake trough (a & d), mean wake (b & e) and wake peak (c & f).

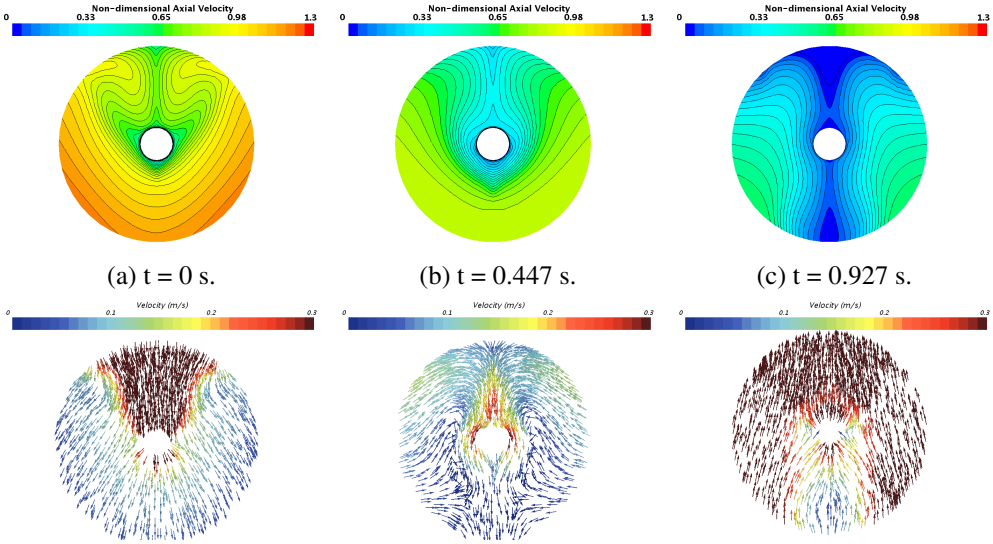

(a) t = 0 s. (b) t = 0.447 s. (c) t = 0.927 s.

(d) t = 0 s. (e) t = 0.447 s. (f) t = 0.927 s.

Fig. 6: Non-dimensional axial velocity contours and transverse velocity vectors for Case 3 at three time instances; wake trough (a & d), mean wake (b & e) and wake peak (c & f).

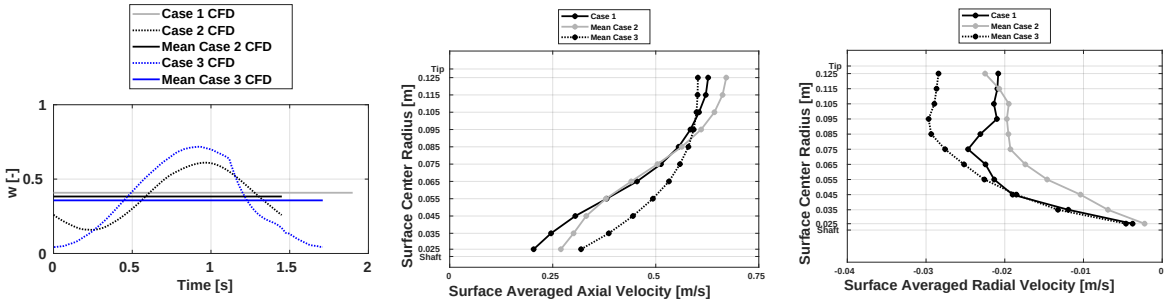

(a) Wake change. (b) Axial velocity. (c) Radial velocity.

Fig. 7: Variation of wake (a) and the mean surface averaged velocity components (b) and (c).

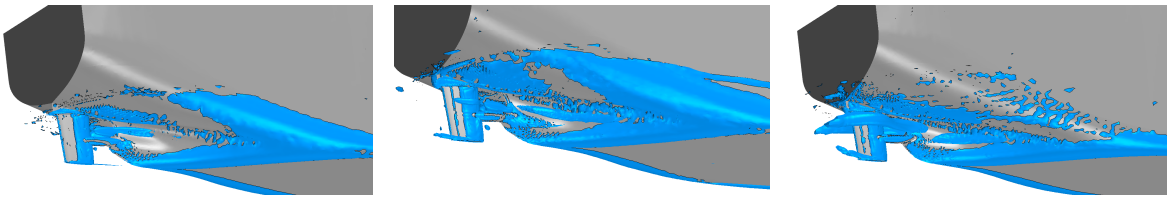

(a) Case 1. (b) Case 2 at t = 0.243 s. (c) Case 3 at time = 0 s.

Fig. 8: The bilge vortex found by Q-criterion = 7.5.

6 Conclusion

This is an ongoing research and so far we have managed to set up a robust method for capturing the dynamics of a ship wake field. The future plan is to investigate the correlation between the ship motions and the wake dynamics more in detail. As a complementary approach to what we have carried out so far, we plan to study the isolated effects from the waves as well as the ship motions on the flow into propeller.

Acknowledgements

This research is funded by The Swedish Transport Administration through LIGHTHOUSE (Swedish Maritime Competence Center). The simulations were performed on resources at Chalmers Centre for Computational Science and Engineering (C3SE) as well as National Supercomputer Center at Linköping University (NSC) provided by the Swedish National Infrastructure for Computing (SNIC). The Maritime Research Institute Netherlands (MARIN) is acknowledged for providing the experimental data.

References

B. Taskar, S. Steen, R.E. Bensow, and B. Schröder (2016). Effect of Waves on Cavitation and Pressure Pulses. *Journal of Applied Ocean Research*, **60**, 61–74.

M. Irannezhad, A. Eslamdoost and R.E. Bensow (2019). Numerical Investigation of a large diameter propeller Emergence Risk for a Vessel in waves. Proceedings of the 8th International Conference on Computational Methods in Marine Engineering (MARINE 2019), Gothenburg, Sweden.

M. Peric' (2017). Best Practices for Simulations With Waves. Presentation at STAR Global Conference, Berlin, Germany.

Muzaferija, S and Peric', M. Computation of free surface flows using interface-tracking and interface-capturing methods. *In Nonlinear water wave interaction*, pp. 59–100, Southampton: WIP Press, (1999).

International Towing Tank Conference (ITTC). Practical Guidelines for Ship CFD Applications. In: *Proceedings of the* 26th *ITTC*, (2011).